

Mechanical-cellular electrical conversion model reshapes the immune microenvironment of peripheral nerve by modulating neutrophil extracellular traps

Yaowei Lv¹, Xiangyun Yao², lei Zhan³, Jinye Shi², Xiangyang Wang⁴, Hede Yan⁴, Xu Wang², Chen Huang³, Yun Qian¹, and Yuanming Ouyang²

¹Shanghai Sixth People's Hospital

²Shanghai 6th Peoples Hospital Affiliated to Shanghai Jiaotong University School of Medicine Department of Orthopaedic Surgery

³Donghua University

⁴The Second Affiliated Hospital and Yuying Children's Hospital of Wenzhou Medical University

May 02, 2024

Abstract

Perturbations of the immune homeostasis following peripheral nerve injury (PNI) disturbs growth microenvironment that delays nerve repair. Although extensive efforts have been made to stimulate nerve regeneration, their efficacy is limited by energy deficiency and persistent and overactive inflammation. It is not yet clear how exogenous implantable neural electrical stimulation system regulates immune homeostasis and promotes peripheral nerve regeneration. Here reports a self-powered immunoactive scaffold based on piezoelectric and electroconductive materials. Such in situ electrical stimulation technique regulates lasting and high-level inflammatory cytokines infiltrated in injured nerve tissue, modulates aberrant neutrophil activities and promotes fast revascularization. By benefiting immune balance and angiogenesis, this electroactive scaffold averts growth-suppression following PNI and robustly facilitates neural regeneration. Therefore, this piezoelectric model represents an effective tool for PNI immunotherapy.

Mechanical-cellular electrical conversion model reshapes the immune microenvironment of peripheral nerve by modulating neutrophil extracellular traps

Yaowei Lv^{a,b,1}, Xiangyun Yao^{a,1}, Lei Zhan^{c,1}, Jinye Shi^{a,b,d,1}, XiangYang Wang^e, Hede Yan^e, Xu Wang^{a,b}, Chen Huang^{c,***}, Yun Qian^{a,b,**}, Yuanming Ouyang^{a,b,*}

a National Center for Orthopedics, Department of Orthopedics, Sixth People's Hospital Affiliated to Shanghai Jiao Tong University School of Medicine, Shanghai, 200233, China;

b Shanghai Engineering Research Center for Orthopaedic Material Innovation and Tissue Regeneration, Shanghai, 200233, China;

c State Key Laboratory for Modification of Chemical Fibers and Polymer Materials, College of Textiles, Donghua University, Shanghai, 201620, China

d College of Fisheries and Life Science, Shanghai Ocean University, Shanghai, 201306, China

e Department of Orthopaedics, The Second Affiliated Hospital of Wenzhou Medical University, Wenzhou, 325003, China.

1 These authors contributed equally to this work.

Keywords

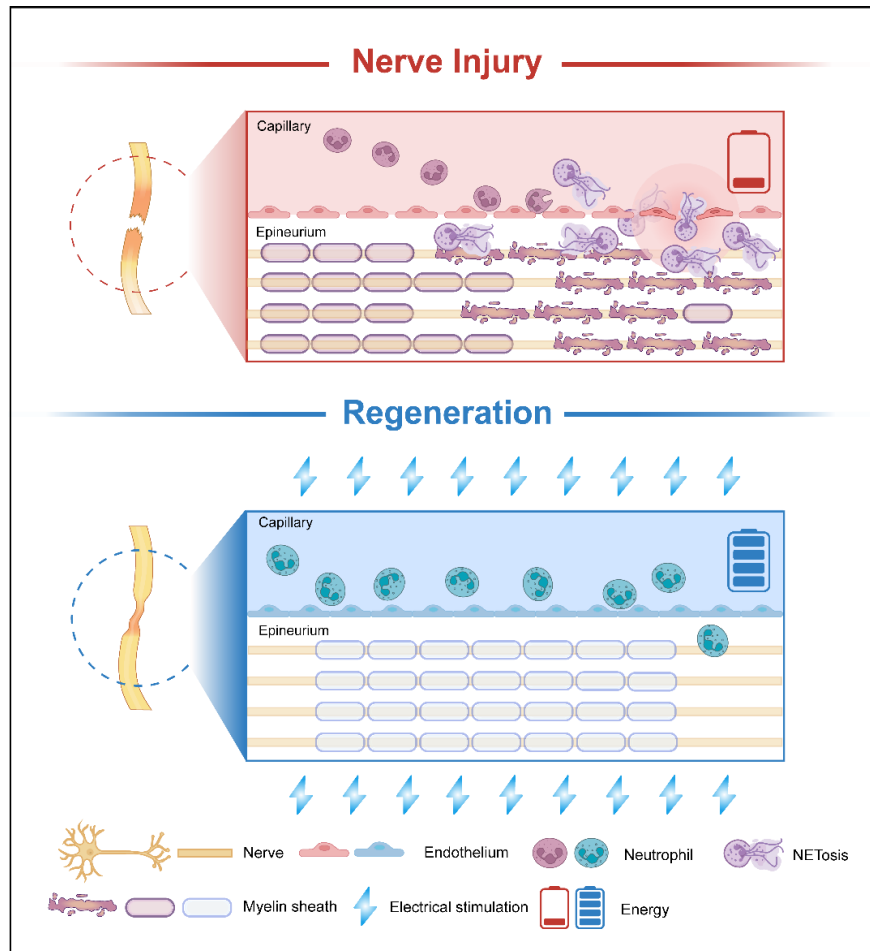
piezoelectricity, piezoelectric nanogenerator, angiogenesis, peripheral nerve regeneration, tissue engineering

Abstract

Perturbations of the immune homeostasis following peripheral nerve injury (PNI) disturbs growth microenvironment that delays nerve repair. Although extensive efforts have been made to stimulate nerve regeneration, their efficacy is limited by energy deficiency and persistent and overactive inflammation. It is not yet clear how exogenous implantable neural electrical stimulation system regulates immune homeostasis and promotes peripheral nerve regeneration. Here reports a self-powered immunoactive scaffold based on piezoelectric and electroconductive materials. Such *in situ* electrical stimulation technique regulates lasting and high-level inflammatory cytokines infiltrated in injured nerve tissue, modulates aberrant neutrophil activities and promotes fast revascularization. By benefiting immune balance and angiogenesis, this electroactive scaffold averts growth-suppression following PNI and robustly facilitates neural regeneration. Therefore, this piezoelectric model represents an effective tool for PNI immunotherapy.

Highlights

- The optimal electrical stimulation parameters for neural regeneration were identified.
- The electrical stimulation model can enhance rapid vascularization of endothelial cells and provide them with energy.
- Electrical stimulation may reshape the immune microenvironment by regulating the formation of neutrophil extracellular traps (NETs)



Graphical abstract

A summary diagram of the mechanisms by which peripheral nerve conduits promote nerve repair. Self-generated piezoelectric nanofilms produce micro-currents. The neutrophil senses electrical stimulation and breaks down the extracellular trap, which promotes nerve reconstruction.

1. Introduction

The repair of nerve injuries remains a challenging issue in clinical treatment[1]. Electrical stimulation proved effective in promoting nerve regeneration in clinical practice[2, 3]. However, current applications face several challenges: 1) The frequency and amplitude of exogenous electrical stimulation, which are crucial for peripheral nerve regeneration, are difficult to control. In clinical settings, high electric currents often lead to complications such as pain, electrical injuries, and psychological trauma[4]. 2) The intrusive power supply equipment is bulky, difficult to replace, has a short lifespan, and may trigger immune rejections[5]. 3) Invasive electrodes produce electrical stimulation to cells at the injury site, which is uncontrollable[6, 7]. Ideally, an implantable neural electrical stimulation system should be controllable and compatible with neural preferences.

Piezoelectric materials offer an in-built power source for peripheral nerve repair[8, 9]. The advancement of pliable materials, which convert passively generated mechanical energy into electrical energy, is crucial for

sustainable energy production. This kind of mechanical energy can be generated by muscle contractions, produced either by the autonomic nervous system, or the body's self-regulating cells [10]. However, harnessing this energy is often challenging as the placement of implanted electrodes in areas such as the heart, aorta, and mediastinum typically necessitates open-heart surgery. This often leads to significant trauma, postoperative infections, and inevitable immune rejection[11]. Skeletal muscle contracture usually results in limited mechanical deformation, which restricts the generation of adequate nerve electrical stimulation signals from the implanted piezoelectric material and impedes nerve regeneration[12]. Following PNI, various cells within the nerve tissue attempt to migrate across the nerve stump[13]. Intriguingly, these minute cell-level deformations, when acted upon by piezoelectric materials, can generate electrical signals that are sufficiently reactive to excitable cells[14]. To generate ample electrical stimulation *in vivo*, bioactive materials must leverage small deformations to produce electrical signals that can sufficiently stimulate nerve electrical excitation[15]. Indeed, enhancing the piezoelectric, ferroelectric, and dielectric properties of biomaterials has been a focal point in nerve repair tissue engineering[16].

Polyvinylidene fluoride (PVDF) is favored for its easy preparation, excellent mechanical flexibility, and good biological safety. It has become a prominent component of piezoelectric materials and a popular type of biomaterial in the field of tissue engineering[17]. The molecular chain of PVDF contains a strongly electronegative fluorine atom, thus providing a remarkable dipole moment. Among the five crystalline polymorphic forms of PVDF, the β phase has exceptional piezoelectric properties[18]. However, the stiffness and piezoelectric coefficient (D33) of conventional PVDF are less than those of crystalline or ceramic piezoelectric materials. Various methods have been developed to increase the piezoelectric properties of PVDF, such as co-polymerization with other polymers, incorporation of nanoparticles, mechanical drawing, annealing, or polarization. All these methods promote the formation of β phase in PVDF[19]. PVDF is frequently co-polymerized with trifluoroethylene (TrFE). The piezoelectric efficiency of the P (VDF-TrFE) copolymer is not constant and depends on the factors including the copolymer content, the loading mechanical force and the loading frequency[20]. The addition of fluorine atoms expands the chain spacing and reduces the phase transition activation energy, encouraging the transition from α phase to β phase without mechanical stretching[21]. Nanoparticles such as zinc oxide[22], graphene oxide[23] and barium titanate[24] can effectively induce β -phase formation. The addition of these nanoparticles as nucleating agent can effectively promote the formation of β phase in PVDF. Lastly, the synthesis process, such as the synthesis temperature and the electrospinning conditions, may also affect the formation of β phase.

The disruption of the immune microenvironment following PNI often serves as a significant barrier to nerve regeneration[25]. In clinical contexts, our understanding of the cellular and molecular mechanisms that underpin immune cell responses to these disruptions remain limited. Most of the existing focus has been on the immune reprogramming of macrophages[26-28]. Neutrophils, the most abundant immune cells in human peripheral blood, are the first to arrive at sites of tissue damage[29]. These cells combat infection and inflammation through a variety of processes, including intracellular degradation, extracellular digestion, and extracellular entrapment[30]. However, the specific role of neutrophils in the context of PNI remains largely undefined.

In this study, we designed a piezoelectric conductive composite nerve scaffold. The complex activity of cell migration generates minute deformations on the scaffold surface, which in turn leads to the creation of electrical signals. These signals play a crucial role in regulating cellular metabolism and biological behavior. The generated microcurrents have been observed to limit the excessive inflammatory response of neutrophils following PNI, thereby promoting the regeneration of the damaged peripheral nerve tissue (Fig 1). Moreover, nerve conduits fabricated from piezoelectric materials exhibit excellent mechanical and electrical properties, as well as dependable biological safety. Following three months of *in vivo* animal experimentation, the nerve conduits demonstrated significant efficacy in facilitating nerve repair. Given the premise of biological safety, the electrophysiological evaluation outcomes of the nerve conduits, coupled with their ability to promote angiogenesis, were found to be comparable with those achieved through autologous nerve transplantation.

2. Results

2.1. Excessive neutrophil after PNI inhibits nerve regeneration.

After peripheral nerve damage, the bioelectrical signal is immediately interrupted. The immune system responds vigorously in real time. To investigate the effect of early immune response following acute nerve injury, we established a model of peripheral nerve transection and conducted a preliminary experiment without any intervention. According to prior research, neutrophils in the rats were the initial immune cells to arrive at the injury site within a span of 6-8 hours, reaching a peak approximately at the 12-hour mark. After a period of 1-2 days, neutrophils completed their homing reaction, following which, their count steadily decreased to a low level[31]. Consequently, we decided to analyze the degree of inflammation and cellular status in both injured and normal nerves, at 12 hours post-injury.

To measure the inflammation level subsequent to nerve transection without any treatment, we employed histopathology and immunofluorescence assays (Figure 2A-B). Upon examining the longitudinal section of the proximal part of the sciatic nerve injury, we observed an aggregation of neutrophils in the early phase of injury (Figure 2C). These neutrophils were primarily located in the epineurium, exhibiting an increased aggregation closer to the injury site (Figure S1), which foreboded that immune system managing to redeem the disturbed immune microenvironment and start regenerate programs. Similar outcomes were drawn from MPO immunofluorescence experiment (Figure 2D).

C-caspase 3 acts as an early signifier of nerve damage, whereas KI67 serves as an indicator of initial nerve tissue repair. We assessed the metabolic variations in the injured nerve through measuring the expression levels of both C-caspase 3 and KI67 in the damaged and the normal nerves (Figure 2 E-F). According to *in vivo* immunofluorescent images, the elevated C-caspase 3 signifies injury and apoptosis in a greater number of nerve-related cells, while the rise in KI67 suggests that nerve repair commences at the injury's initial phase (Figure 2G-H). The immunofluorescence results of IL-1, IL-6, and TNF- α also reported the immune disorder of the nerve after injury (Figure 2I-O). To investigate the impact of neutrophil NET on neuronal metabolism, we conducted *in vitro* experiments, excluding the interference of other cells. The activated neutrophil by Phorbol 12-myristate 13-acetate (PMA) released an abundant amount of NET, leading to reduced proliferation and increased apoptosis in Schwann cells (Figure 2P, Figure S2). Prior research has demonstrated that excessive activation of NET considerably hampers tissue repair[32], and that diminishing its expression aids in inflammation control[29]. Similarly, the regulation of skeletal proteins through electrical stimulation can influence the migratory ability of cells[6]. we aim to apply this stimulation to the regulation of immune cells. In conclusion, the aforementioned experiments confirmed the conversion of the immune state in nerve tissue during the early injury phase, and this disruption exhibited a regulable function.

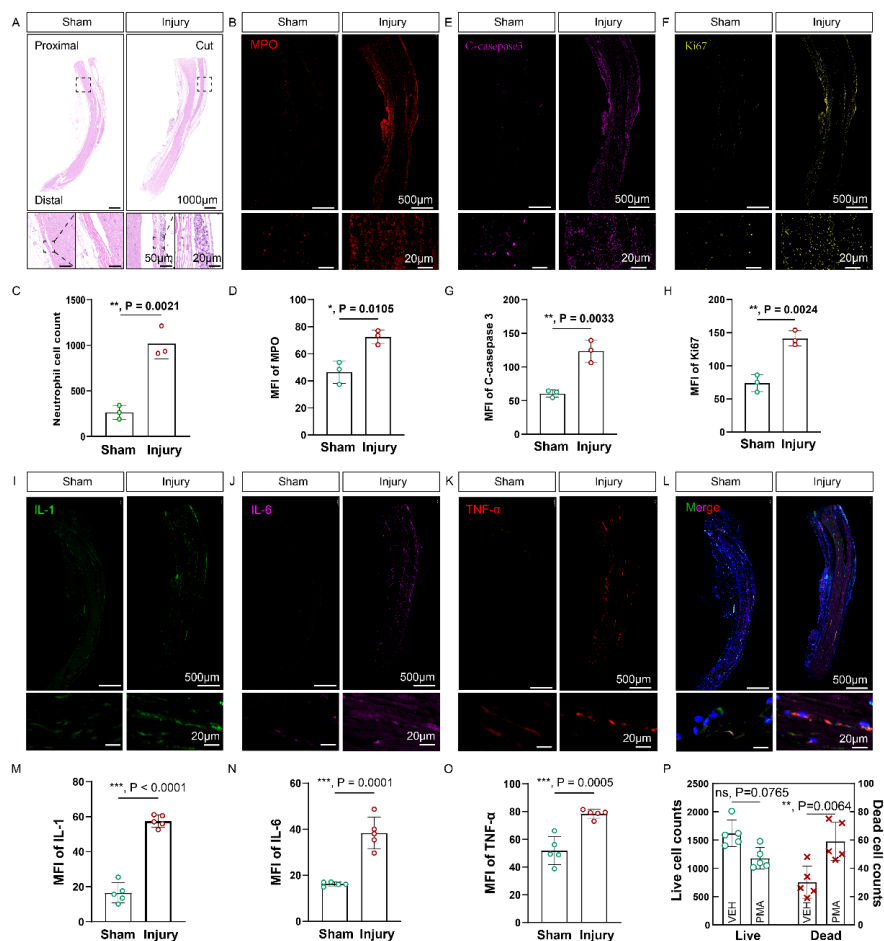


Figure 1. Increased neutrophil infiltration of the damaged nerve. (A) HE staining of Sciatic nerve in the longitudinal section with or not with injury. Scale bars=1000 μm ; 50 μm ; 20 μm (B) Myeloperoxidase (MPO) immunofluorescent staining image of the nerve. Scale bars=500 μm ; 20 μm (C) Quantitative analysis of the number of neutrophil cells in the epineurium. (D) Mean fluorescent intensity (MFI) of MPO positive cell. (E) Immunofluorescence staining for C-caspase-3 in Sciatic nerve. (F) Immunofluorescence staining for Ki67 in Sciatic nerve. (G) MFI of C-caspase 3 positive cell. (H) MFI of Ki67 positive cell. (I) Immunofluorescence staining for IL-1 in Sciatic nerve. (J) Immunofluorescence staining for IL-6 in Sciatic nerve. (K) Immunofluorescence staining for TNF- α in Sciatic nerve. (L) Merged images of inflammatory markers from I to K. (M) MFI of IL-1 positive cell. (N) MFI of IL-6 positive cell. (O) MFI of TNF- α positive cell. (P) Quantitative analysis of live dead cells analysis.

2.2. The P(VDF-TrFE)/rGO/PCL nerve conduit converted mechanical electrical signals into cellular electrical signals.

Can tissue engineering scaffolds be used as regulator for interrupted nerve current signals? It has been documented that piezoelectric materials can influence cell behavior and viability via microcurrents created by mechanical deformation[6, 14]. In an attempt to restore the microenvironment of nerve regeneration disturbed in the early injury phase, we developed a piezoelectric conductive composite scaffold to ascertain whether it can modulate the aforementioned inflammatory process. We have fabricated fiber films of varying concentrations using electrospinning.

We employed electrospinning technology to fabricate three types of films (rGO/PCL (rP), 10%P (VDF-

TrFE)/rGO/PCL (10% PrP) and 20%P (VDF-TrFE)/rGO/PCL (20% PrP)), which were subsequently folded into tubular scaffolds for peripheral nerve regeneration (Figure 2A). The electrospun fibers exhibited a relatively uniform morphology, and the incorporation of rGO did not alter the fiber morphology (Figure 2B). Moreover, rGO was uniformly loaded onto the fiber surface. The initial modulus of all three scaffolds were comparable. Notably, when P (VDF-TrFE) content reached 10%, the resultant film displayed the highest initial modulus (Figure 2C). Interestingly, the addition of P (VDF-TrFE) enhanced crystallinity of electrospun fibers, indicating that PrP possessed superior piezoelectric properties (Figure 2D). It is worth mentioning that due to the low concentration of rGO used in this study, its characteristic peaks could not be detected by Fourier-transform infrared spectroscopy (FTIR, Figure 2E), which was consistent with previous research findings^[33]. Due to the hydrophobic nature of rGO and P (VDF-TrFE), remarkable hydrophilicity was observed among rP, 10% PrP and 20% PrP films, and the blended films remained hydrophobic as well (Figure 2F). Intriguingly, when identical small loads were applied, both 10% and 20% PrP films generated similar voltages that were significantly higher than those produced by rGO/PCL film, and thereby confirming excellent piezoelectricity conferred by P (VDF-TrFE) (Figure 2G-I). To further evaluate the electrical characteristics of P (VDF-TrFE)/rGO/PCL conduits, we tested the dielectric spectrum and dielectric loss of fiber (Figure 2J-K). In order to ascertain the impact of the current produced by these materials on neutrophils, we evaluated the intracellular calcium levels in neutrophils exposed to different materials. Flow cytometry results demonstrated that the 10% PrP membrane significantly augmented the calcium influx in cells compared to other groups (Figure 2L).

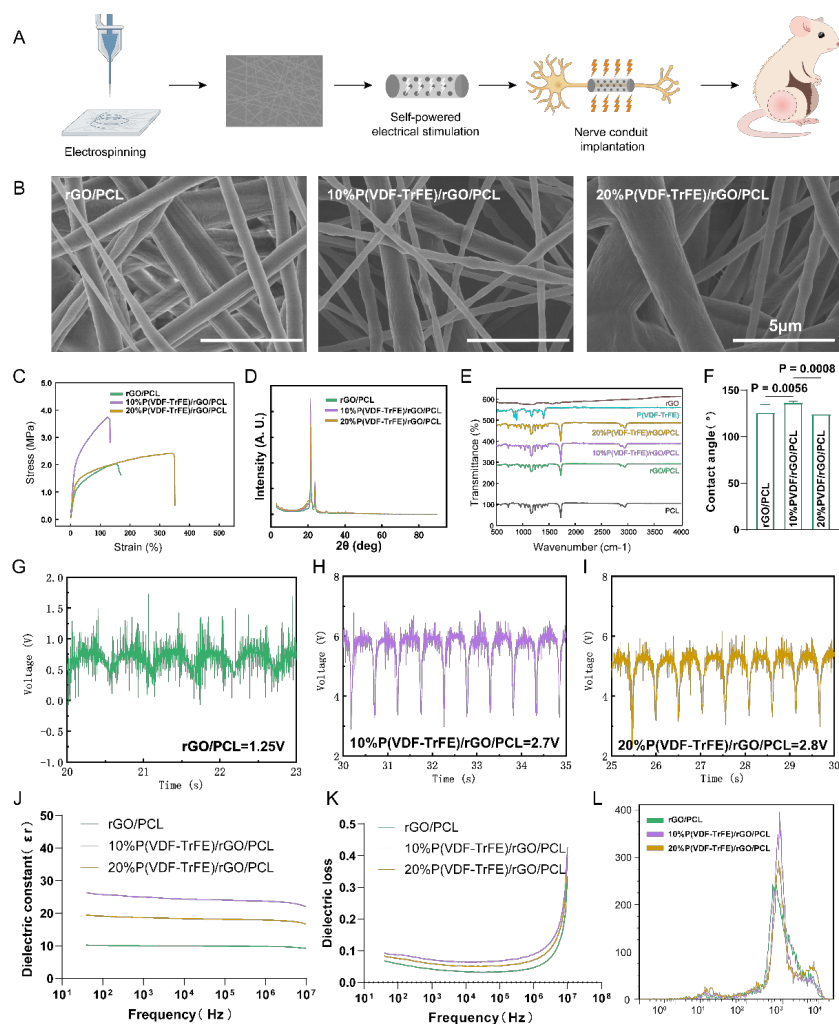


Figure 2. Fabrication and performance analyses of materials. (A) Schematic diagram of electrospinning material preparation. (B) Scanning electron microscopy (SEM) of fibrous membranes. Scale bars=5 μm (C) Stress-strain curves of nerve conduits. (D) X-ray diffraction patterns. (E) Fourier transform infrared spectroscopy. (F) Water contact angle. Electro-mechanical conversion analysis of (G) rGO/PCL, (H) 10%P (VDF-TrFE) /rGO/PCL and (I) 20%P (VDF-TrFE)/rGO/PCL. (J) Dielectric spectrum of nerve conduits. (K) Dielectric loss of nerve conduits. (L) Intracellular calcium transients induced by different conduits.

2.3. The cellular electrical signals generated by piezoelectric materials promote the rapid vascularization of endothelial cells.

What are the electrical stimulation parameters suitable for neurovascularization? In our previous experiments, we determined that the optimal concentration of reduced graphene oxide (rGO) is 2% [34]. To explore the ideal concentration of Copolymer P (VDF-TrFE) in composite piezoelectric scaffolds, we integrated 0, 10% and 20% P (VDF-TrFE) into 2% rGO/PCL scaffolds and seeded cells onto the surface. Schwann cells and endothelium, integral to peripheral nerve repair, were thus chosen for the experiment with RSC96 and human umbilical vein endothelial cells (HUVEC) to examine the biocompatibility and functionality of PrP. Flow cytometry results indicated no significant difference in the number of apoptotic Schwann cells cultured across varying concentrations of the copolymer (Figure 3A). Cell Counting Kit-8 (CCK8), a widely used method for evaluating cytotoxicity and proliferation, showed an increase in OD value as cell proliferation increases, darkening the solution. After intervals of 6H, 12H, 24h, and 48h, CCK8 results indicated that scaffolds with 10% copolymer were less toxic than those in the other two groups (Figure 3B).

Insufficient intraneuronal vascularization can affect peripheral nerve regeneration [25]. To assess the angiogenic activity associated with different concentrations of PrP, we conducted a Transwell test, a tube formation test, and evaluated mitochondrial membrane potential in HUVEC cells. The Transwell results indicated that the migratory ability of cells in the 10% PrP group surpassed that of the other two groups (Figure 3C-E). Interestingly, despite the 10% PrP group having a lower migratory ability than the control group, its angiogenic capacity exceeded that of the normal group in the tube formation experiment (Figure 3F-J). This implies that 10% PrP may enhance angiogenesis by coordinating endothelial cell functions, rather than simply boosting the migration ability (Figure 3K). The mitochondrial membrane potential experiment exhibited a similar pattern (Figure 3L-N).

These findings suggest that 10% PrP demonstrates relatively low cytotoxicity and a robust capacity for promoting angiogenesis and preserving endothelial mitochondrial energy. Consequently, we selected 10% PrP as the material for further *in vivo* biosafety and efficacy evaluations. Unless otherwise specified in subsequent content, all references to PrP refer to 10% p (VDF-TRFE)/rGO/PCL nerve conduits.

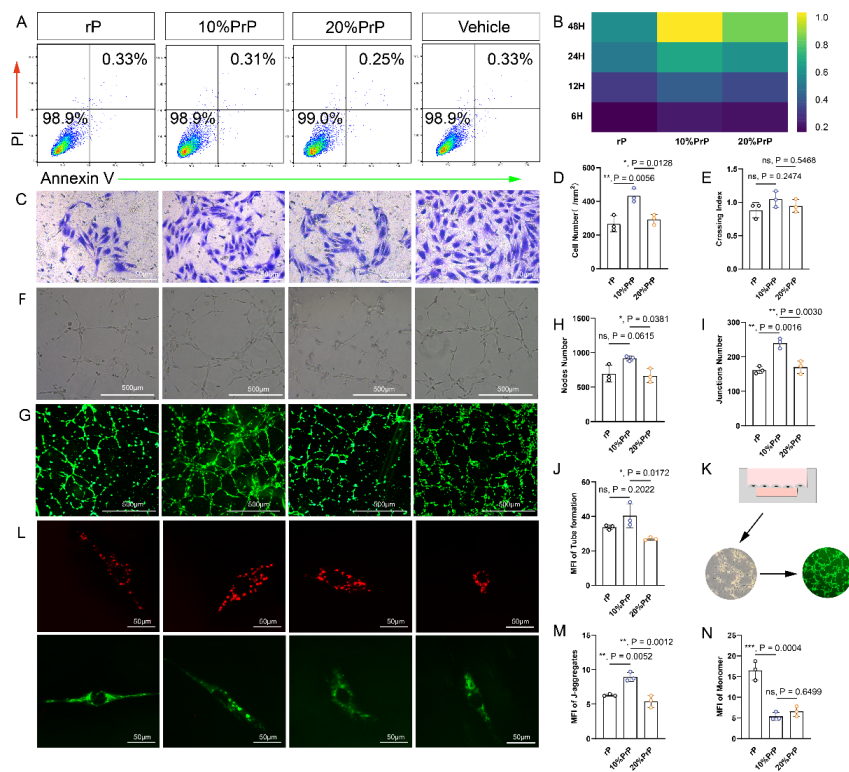


Figure 3. Evaluation of P (VDF-TrFE)/ rGO/ PCL nerve scaffolds *in vitro*. (A) Apoptosis of Schwann cells measured by flow cytometry (B) Cell Counting Kit-8 (CCK-8) experiment. (C) Assessment of cell migration ability. Scale bars=50 μ m (D) Quantitative analysis of cell number passing through Transwell pores (E) Quantitative analysis of the crossing index of the Migration Experiment (F) Angiogenic experiments under bright field and (G) fluorescent microscope. Scale bars=500 μ m (H) Quantitative analysis of the nodes number of the angiogenic experiment. (I) Quantitative analysis of the junction number in angiogenic experiment. (J) Quantitative analysis of the MFI of calcein. (K) The illustration of angiogenesis experiment (L) Mitochondrial membrane potential assay kit with JC-1. Scale bars=50 μ m (M) Quantitative analysis of the mean fluorescence intensity of activated and (N) inactivated mitochondria measured by mitochondrial membrane potential.

2.4. 10% p (VDF-TRFE)/rGO/PCL nerve conduits promote the recovery of damaged Sciatic nerve in a biologically safe manner *in vivo*.

Ensuring the biosafety of neural implants in tissue engineering is crucial. We verified the organ and metabolic toxicity of nerve conduits by implanting them into rats for a period of three months and monitoring organ and blood homeostasis. Pathological changes were absent in tissues of the heart, liver, spleen, kidneys, and lungs (Figure S3A). Confirmation of organ and hematology biosafety was achieved through tests of liver and kidney function, as well as electrolyte levels. Additionally, a blood test was conducted (Figure S3B). The results demonstrated that the PrP conduit exhibited robust biosafety, aligning with previous *in vitro* safety tests, thus supporting further validation.

To evaluate whether electrical stimulation via our custom-designed nerve conduits can promote peripheral nerve regeneration, we conducted a series of experiments *in vivo*. We initiated our study by assessing neuromuscular recovery in rats through a series of behavioral tests. Specifically, we trained the rats to navigate from one end of the track to the other. The shape and pressure of their footprints were recorded using pressure-sensitive acrylic plates (Figure 4A), a well-established method for analyzing motion recovery [35]. We observed that the poorer the nerve recovery, the more indistinct and elongated the footprint

appeared, and the less pressure was exerted by the foot (Figure 4B-C). Our results revealed that the nerve recovery in rats treated with 10% PrP paralleled that of autologous nerve transplantation (Figure 4D), with a significant increase in footprint pressure (Figure 4E).

Following this, we proceeded to evaluate nerve conduction. Under anesthesia, the rats were incised along the initial cut to reveal the nerve. One electrode was introduced into the gastrocnemius muscle, while the other was used to stimulate both ends of the nerve defect, allowing us to evaluate the axonal and myelin functionality of the nerve. Our data indicated that the neural function in rats treated with 10% PrP had recuperated to a level comparable to autologous nerve transplantation (Figure 4F-H). We subsequently harvested the sciatic nerves and performed histological staining, immunofluorescence, and transmission electron microscopy experiments to quantitatively observe the nerve recovery (Figure 4I-K). The results demonstrated that this specially designed piezoelectric material effectively promoted the regeneration of the myelin sheath (Figure 4L-N). Histological sections of gastrocnemius muscle tissues further bolstered our findings (Figure 4O). In summary, this piezoelectric material can promote regeneration after PNI.

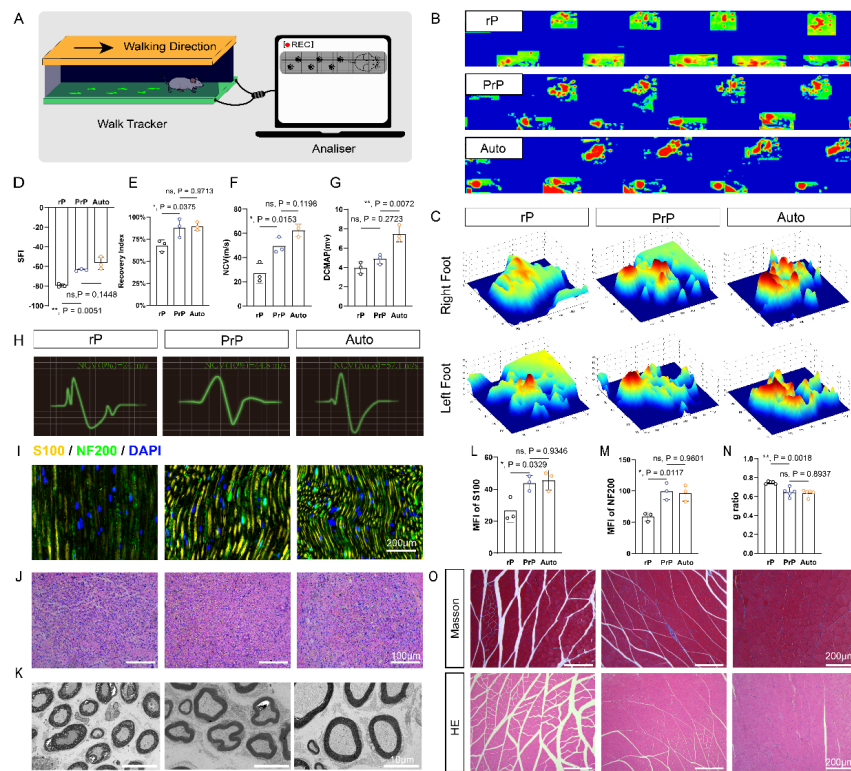


Figure 4. The neuromuscular recovery was observed after 3 months. (A) A schematic of behavioral analysis. (B) Rats walking footprints. (C) The pressure of each hind foot on the board. (D) Quantitative analysis of Sciatic nerve index. (E) Quantitative analysis of pressure recovery index. (F) Quantitative analysis of nerve conduction velocity (NCV) and (G) distal compound motor action potential (DCMAP) (H) Action potential waveform of the Sciatic nerve (I) Immunofluorescence staining for S100 and NF200 in sciatic nerve. Scale bars=200 μm (J) HE staining of the Sciatic nerve. Scale bars=100 μm (K) Representative electron micrographs of sciatic nerve cross sections. Scale bars=10 μm (L) MFI of S100 positive cell. (M) MFI of NF200 positive cell. (N) Analysis of myelin sheath thickness by calculation of the g-ratio. (O) Masson and HE staining of gastrocnemius. Scale bars=200 μm

2.5. Piezoelectric stimulation works to repair damaged nerves by inhibiting NET and promoting rapid vascularization.

How does overactivated NET in the early stage of PNI affect regeneration in the long term? We undertook preliminary animal studies to evaluate the influence of early neutrophil activity on neurological recovery. Generally, we implanted various materials into the cut nerve. After a span of 12 hours post-injury, we extracted the nerves to check their impact on the neutrophil. HE staining hinted that the nerve repair effect could potentially be obtained by manipulating neutrophil behavior (Figure 5A). Following this, we detected Histone H3 (HH3) and myeloperoxidase (MPO) (Figure 5B), specific markers indicating the presence of neutrophil extracellular traps (NETs), and CD31, specific markers indicating the occurrence of angiogenesis (Figure 5C). Our findings revealed a substantial expression of extracellular NETs in the rP group, but the NETs' expression in the PrP and autologous transplantation groups was over 1.5 times lower (Figure 5D-E). The nerves subjected to electrical stimulation have more granulation tissues, indicating a higher degree of vascularization (Figure 5F). *In vitro* results mirrored these findings. In essence, we isolated rat peripheral blood neutrophils, cultured them on different materials, and then detected NET expression using Western blot (Figure 5G-H). Further, we co-cultured endothelial cells with neutrophils treated with varied materials and conducted a scratch assay (Figure 5I). The data showed a superior outcome in the PrP group compared to the rP group, and strikingly, the effect of the PrP group was nearly identical to the non-activated neutrophil group on endothelial cells (Figure 5J). Interestingly, when we explored the correlation between this early immune regulation and long-term tissue repair, macrophages showed an interesting adjustment. (Figure 5K.) The M1 polarization of macrophages decreased in the nerve conduits with early electrical treatment. (Figure 5L-M) These results suggest that electrical stimulation could regulate the immune response in the early stage of injury, enhancing angiogenesis and nerve regeneration, and the early inflammatory regulation may indicate an increase in the benefits of long-term immune microenvironment-mediated nerve regeneration.

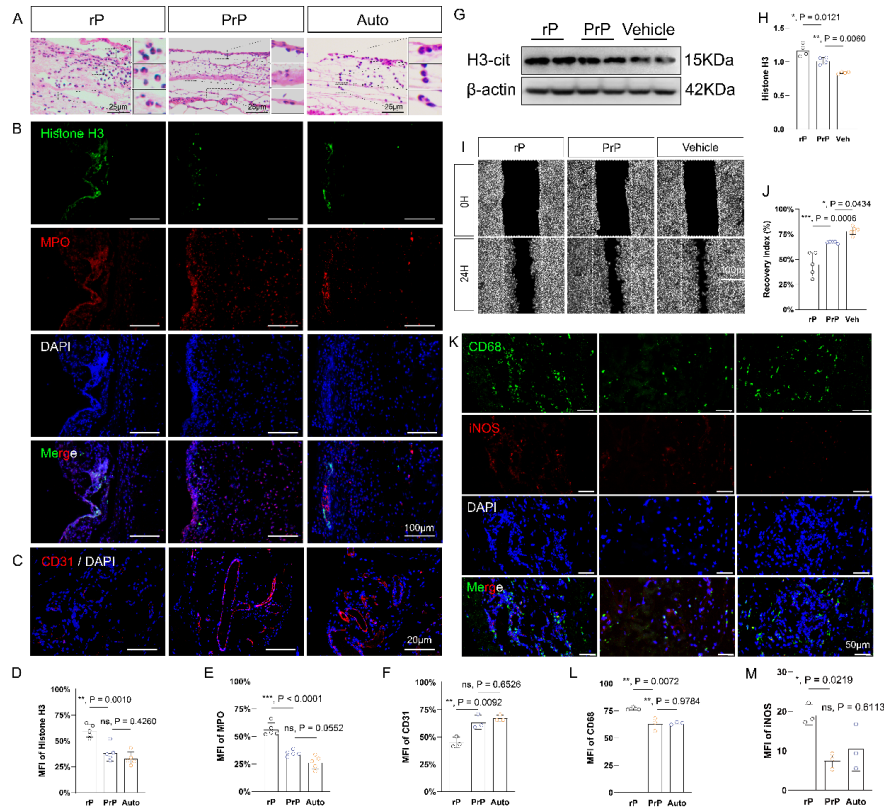


Figure 5. Nerve conduits regulated neutrophil behavior. (A) The neutrophil in the epineurium. Scale bars=25 μ m (B) Histone H3 and myeloperoxidase immunofluorescent staining of regenerative nerves. Scale bars=100 μ m (C) Immunofluorescence staining for CD31 in sciatic nerve. Scale bars= 20 μ m (D) Quantitative

analysis of the mean fluorescence intensity of Histone H3. (E) Quantitative analysis of the mean fluorescence intensity of MPO. (F) Quantitative analysis of the mean fluorescence intensity of CD31. (G) Western blot analysis of Histone H3 expression in neutrophil. (H) Relative expression levels of Histone H3. (I) Wound-Healing Assay after co-culture of neutrophil and endothelial cells. Scale bars=100 μm (J) Quantitative analysis of the repair index of endothelial cells. (K) Immunofluorescence staining for CD68 and iNOS in sciatic nerve. Scale bars= 50 μm (L) MFI of CD68. (M) MFI of iNOS.

3. Discussion

Increasing attention has been paying to the impact of implant bioelectricity on tissue repair, particularly regarding the generation and maintenance of bioelectricity in peripheral nerve tissue engineering[36]. It has been observed that reconstructing the normal electrophysiological microenvironment can significantly facilitate the repair of injured sites or wound tissue[37] Consequently, numerous methods of energy substitution are being explored. Ultrasound stimulation, often utilized as a source of mechanical stress *in vitro*, is one such method[21]. Biomaterials have even been found to stimulate nerve repair by generating currents in response to changes in an external magnetic field[38]. However, these stimuli can be cumbersome and challenging to convert for tissue repair purposes. For instance, nerve damage patients are often required to be exposed frequently to an electric field for brief periods, ranging from seconds to minutes[39]. Piezoelectric materials offer a promising solution. They have been demonstrated to promote tissue regeneration via *in situ* electrical stimulation, independent of exogenous mechanical friction electrical stimulation as a power source[2, 10, 37]. Endothelial and immune cells can cause minute deformations on these materials, which can generate sufficient electrical signals to modify cellular metabolism[14, 40]. Research has shown that the electrical stimulation from piezoelectric materials may serve as an internal generator for peripheral nerve regeneration[41]. For example, electrospinning scaffolds composed of P (VDF-TrFE)/BaTiO₃ nanoparticles, as established by NUNES-PEREIRA J [42], can generate voltages up to 5.02 V and 25 mW of power under mechanical stimulation. This provides robust electrical support for the recovery of injured nerves.

The preparation of ZnO/PCL piezoelectric composite scaffolds was successful, demonstrating remarkable properties for neural recovery[41]. These endogenous piezoelectric materials were found to prompt the rapid regeneration of a damaged sciatic nerve within a span of 4 weeks. The data suggests that the optimal voltage range to encourage nerve regeneration lies between 0.2 mV and 10 V[43]. Interestingly, the introduction of nanoscale currents in the vicinity of peripheral nerves appears adequate to modify the metabolic microenvironment, thereby facilitating nerve regeneration[44]. However, it is crucial to note that excessive electrical stimulation could prove counterproductive, posing a threat to the cytoskeleton and the cells' migration capacity, which could be harmful to tissue repair[6].

NETs significantly contribute to extracellular DNA that impairs wound healing[32]. They are also known to enhance the migratory capabilities of tumor cells[45], and can foster chemotherapy resistance[46]. Neutrophil over-activation can lead to the transformation of macrophages into M1-type macrophages, thereby intensifying the inflammatory response[47]. Neutrophils secrete chemokines that boost the macrophages' capacity to clear myelin sheaths[48], and simultaneously serve as a backup for Wallerian degeneration, as no notable delay in myelin denaturation is observed post suppressed macrophage activity[49]. This "relay mode" of neutrophil macrophages suggests a potential role of neutrophil signal crosstalk with macrophages in inflammatory responses post nerve injury[50]. Prior research indicates that inhibiting NET formation can encourage the prompt arrival of macrophages at PNI sites, fostering regeneration[31]. Neutrophils are inherently flexible in adapting to environmental signals, not even limited by their initial stage of maturation.[51] This means that neutrophils in the neural regenerative microenvironment may follow the same process, adjusting their own immune function status under the guidance of the nerve guide conduits, and thus transforming into a niche that promotes peripheral nerve repair. Our aim is to regulate NETs through biophysical methods to expedite nerve tissue repair. However, specific mechanism by which piezoelectric materials modulate the behavior of immune cells during the initial phase of inflammatory injury remains

unclear. Excess DNA, a pivotal source of extracellular DNA at injury sites, is often implicated in the cyclic GMP-AMP (cGAS)-Stimulator of Interferon Genes (STING) pathway [52]. Indeed, the activation of this pathway is intricately linked with vascular, neuronal, and interstitial cell injuries [53, 54]. This indicates the feasibility of biomaterials inhibiting the formation of neutrophil extracellular traps to improve cells' regenerative capacity in PNI.

In our research, P (VDF-TrFE) /rGO/PCL emerges as a promising material for nerve regeneration[55]. Prior studies have underscored the advantages of biomimetic materials in facilitating bioelectrical signal transmission during peripheral nerve regeneration[56-58]. An appropriate local voltage potential has the capacity to instigate a conformational shift in the voltage-gated channel, leading to intracellular calcium transients[23]. The in-situ electrical properties of piezoelectric materials are influenced by both the material's form and the magnitude of the cell adhesion force[40]. Reduced graphene oxide, a commendable conductor within the graphene family, can proficiently convey electron flow, thereby enhancing the piezoelectric attributes of the materials[59]. Superior cell adhesion properties when applied to bio-conductive materials can foster more effective mechano-bioelectric signal interactions between the materials and the regenerating cells [40, 60].

While our study demonstrates that piezoelectric fibrous materials modulate neutrophil inflammatory responses during the early stages of nerve injury, potentially aiding nerve regeneration, we need to acknowledge that neutrophil extracellular traps (NETs) are not entirely detrimental to nerve repair. In fact, an optimal concentration of NETs may promote nerve repair. Lower NET concentrations may stimulate cell proliferation via the NF-KB pathway[61]. Recent research has revealed that neutrophil populations with immature leukocyte phenotypes possess neural repair-promoting functions [62]. This has spurred our interest in deciphering the specific microenvironmental changes within neural tissue that enable the functional reprogramming of neutrophils, shifting from patrolling behavior to specialized, tissue-specific tasks[63]. Our study, however, did not definitively determine the ideal NET concentration for nerve regeneration, marking a substantial limitation. Furthermore, the precise electrical stimulation intensity required to yield the optimal NET concentration remains unclear. These questions necessitate further experimental exploration and hold significant implications for our comprehensive understanding of the role piezoelectric materials play in nerve repair.

4. Conclusion

Our research demonstrated that the production of neutrophil NETs could impede early nerve repair post-injury. Consequently, we engineered a piezoelectric conductive composite nerve conduit, specifically a PrP nerve conduit, which targets early-stage neutrophils at the injury site by deploying an electric current generated through physical deformation. This electrical stimulation disrupts NET formation, thereby eliminating barriers to micro-vessel formation and axonal regeneration. PrP has exhibited promising biosafety and efficacy as an intracellular plant following nerve injury. In conclusion, the effectiveness of piezoelectric materials in peripheral nerve repair has been established, and the PrP nerve conduit may present a competitive edge in future translational applications.

5. Materials and method

5.1. Materials

P (VDF-TrFE) Solvne® 250 /P400 (900904, Sigma-Aldrich, USA) was provided by Shanghai Chongjing Biotechnology Co., Ltd., while the reduced graphene oxide from tea polyphenols (XF247, XFNANO, China) and polycaprolactone (P871874, Sigma-Aldrich, USA) were supplied by Shanghai Yasheng Biotechnology. Aceton and N, N-dimethylformamide (DMF) were purchased from Macklin (Shanghai, China).

5.2. Fabrication and characterization of electroactive P (VDF-TrFE)/rGO/PCL scaffolds

P (VDF-TrFE)/rGO/PCL scaffolds were fabricated using the electrospinning method. The copolymer P (VDF-TrFE) (7525), 2%rGO, and 16% PCL were dissolved uniformly in a mixed solvent comprised of DMF and acetone (6:4). This was done in accordance with the optimal spinning conditions as identified in previous reports[21]. The copolymer concentration within the solution was adjusted to 0%, 10%, and 20%. The injection speed was set at 1 ml/h and a DC voltage of 15 kV was applied between the injector and the mould. The collection distance was maintained at 10 cm. Prior to each experiment, the film was cut into a circular piece of the corresponding aperture size using a perforator and then detached from the foil. The membrane was subsequently immersed in 75% ethanol and exposed to ultraviolet light for 1 hour. The material was then air-dried and set aside for future use.

The surface morphology of electrospun films was examined using a Scanning Electron Microscope (SEM). The microstructure of the electrospun fibers was observed at 5kv following a gold spraying treatment of 30 seconds. A tensile apparatus was employed to determine the mechanical properties of the piezoelectric materials, with the stress-strain curves being drawn based on the elastic modulus and elongation at break. The X-ray Diffractometer (XRD) was set with experimental parameters adjusted to 1.542 Å of copper radiation, to characterize the crystal structures of different materials between the angles of 5 to 80 degrees. The Fourier Transform Infrared (FTIR) spectroscopy (NEXUS-670) was used to evaluate the Fourier transform transmittance in the range of 500 cm to 4000 cm. The contact angle of different materials when interacting with water was measured using a Contact Angle Goniometer (OCA15EC, Germany).

5.3. Cell culture

The RSC96 cell line, procured from Zhongqiao Xinzhou (ZQ0154), was cultured in Dulbecco's Modified Eagle's Medium (DMEM, GIBCO, USA), supplemented with 10% Fetal Bovine Serum (FBS, GIBCO) and 1% penicillin/streptomycin solution (GIBCO, USA). Primary Human Umbilical Vein Endothelial Cells were obtained from Seiyue Biotechnology Co., Ltd. (HUVEC-20001, Cyagen), and these endothelial cells were cultured in specialized media (HUVEC-90011, Cyagen). The culturing was conducted at 37°C in a 5% CO₂ incubator.

5.4. Cytotoxicity assay

We employed a cell counting kit-8 (CCK8) (C6005, NCM Biotech, China) to identify the piezoelectric biomaterials with minimal toxicity to Schwann cell growth. Sterilized films were positioned into 24-well plates, and cells were seeded at a density of 2×10^5 into these plates with different materials. Following a 2-hour period, the cells fully adhered to the membrane surface, marking the beginning of the treatment process. Treatment endpoints were established at 6, 12, 24, and 48 hours post the commencement of the treatment. At the conclusion of the treatment, the complete medium was discarded and replaced with basal medium containing 10% CCK8 reagent. After a further 3 hours, the supernatant was gently removed from each well and the absorbance at 450 nm was recorded.

5.5. Apoptosis experiment

We utilized an Annexin-V-FITC/PI apoptosis assay kit (abs50001,absin,China) to assess cell apoptosis following material treatment. Once the Schwann cells on the membrane achieved confluence of over 85%, they were digested with trypsin (sans EDTA), centrifuged, and subsequently resuspended in 250µl of 2% Annexin-V-FITC solution. This was followed by a 15-minute incubation period at room temperature, shielded from light. Prior to the flow cytometry analysis, which was carried out 5 minutes before loading the sample into the machine, a 250µl aliquot of 2% PI solution was added. The flow cytometry analysis was conducted using a FACS celesta (BD, USA).

5.6. Mitochondrial membrane potential experiment

The assessment of mitochondrial depolarization in human umbilical vein endothelial cells was conducted in accordance with the manufacturer's instructions (C2003s, Beyotime, China). Specifically, JC-1 staining solution (5 µg/ml) was introduced into the cell culture dishes, followed by a 20-minute incubation period in the cell incubator. Subsequently, the dishes were washed twice with a buffer solution, then observed under

a fluorescence microscope. The fluorescence intensities were measured at 490 nm and 530 nm excitation wavelengths. It is noteworthy that a higher mitochondrial membrane potential correlates with an increase in red light intensity, whereas a stronger green light intensity indicates the opposite.

5.7. Angiogenesis experiment

HUVECs naturally develop into reticular tubules on the Matrigel surface at elevated concentrations, thereby simulating angiogenesis in living organisms[64]. A volume of 10 μ l of Matrigel® (354234, Corning, USA) at a concentration of 10 mg/ml was evenly spread in the lower compartment of a μ -slide plate (81506, ibidi, German). The upper compartment was then inoculated with a 50 μ l cell suspension at a density of 2×10^5 cells/ml. The setup was incubated and observed after 24 hours. Following the final observation in the bright field, Calcein-AM/PI (C542, Dojindo, Japan) staining was performed for additional observation. Image J software was utilized to count the vascular nodes and branches.

5.8. Transwell cell migration assay

The Matrigel was combined with the basal medium at a ratio of 1:8 and subsequently added to the upper compartment of the Transwell Plate. Endothelial cells were then seeded onto various membranes and incubated for 2-3 days. Following digestion, cells were centrifuged, re-suspended in basic medium, and then inoculated into the upper compartment of the Transwell Plate. Next, complete medium was added to the lower compartment. After a period of 12 hours, the chamber was removed and gently swabbed with a cotton bud to clean the inner side of the upper compartment. The cells were then stained with crystal violet. The Image J software was used to quantify the number and average area of cells that migrated through the chamber.

5.9. Neutrophil extraction

Initially, we collected peripheral blood samples from Rats. Utilizing a peripheral blood neutrophil separation kit (P9200, Solarbio, China), we carefully combined 16 ml of fresh blood samples with an equal volume of AC mixture (liquid A: liquid C at a ratio of 2:1), followed by centrifugation at 700g for 25 minutes. Post-centrifugation, the neutrophils congregated in a layer described as a white mist at the bottom. This cell layer was gently aspirated, rinsed, and subjected to a second centrifugation (250g for 10 minutes). Subsequently, the cells were re-suspended in 1 ml of Lysate and incubated at room temperature for a 5-minute lysis period. After lysis, the supernatant was removed by a further round of centrifugation (250g for 10 minutes). Finally, the cells were re-suspended in a 1640 basal medium before being seeded onto the material.

5.10. Neutrophil purity test

Following each neutrophil extraction, we conducted purity assessments and cell count measurements. Utilizing a water-blocking pen (BC004, Biosharp, China), we placed droplets of the neutrophil suspension onto a glass slide pre-coated with poly-lysine (ZLI-9802, ZSGB-bio, China), after which we dried the slide in a CO₂-free incubator for a period of two hours. The characteristic lobulated nuclei of the neutrophils became identifiable after staining with diff staining solution (G1540, Solarbio, China) or a DAPI-containing tablet (P0131, Beyotime, China).

5.11. Extraction of neutrophil extracellular traps

Using a previously detailed method, neutrophils were extracted from the peripheral blood and neutrophil extracellular traps (NETs) were subsequently isolated[45]. The neutrophil NETs expression inducer, Phorbol 12-myristate 13-acetate (PMA), was procured from MedChemExpress (MCE, America). In brief, we subjected the neutrophils to a 4-hour stimulation using 500 nm PMA, ensuring their complete activation. Upon reaching the designated time point, we discarded the supernatant and gently rinsed the NETs at the base of the dish with chilled PBS, followed by a 10-minute centrifugation at 1000 g, at a temperature of 4 °C. We then collected the cell-free supernatants containing the NETs (DNA-protein complexes) for subsequent experimentation.

5.12. Live-Dead Cell test

We propagated the RSC96 cell line in 6-well plates, maintaining a growth density of 500,000 cells per well. The cells were then treated for 6 hours with either a purified NET solution or PBS. Following this treatment, the immunofluorescence intensity of live and dead cells was measured using Calcein-AM/PI (Solarbio, China).

5.13. Calcium ion flow experiment

We utilized the Fluo-4 Calcium Assay Kit (S1061s, Beyotime, China) to evaluate the calcium influx in neutrophils post-treatment. The harvested neutrophils were positioned in orifice plates either with or without materials. Following a 6-hour treatment period, the cells were transferred into a centrifuge tube and subjected to fluo-4 staining solution. The levels of calcium influx within the cells were subsequently measured using flow cytometry.

5.14. Wound-Healing Assay

Neutrophils treated with various piezoelectric films were centrifuged, and the supernatant was meticulously collected. A 200 μ l Spear tip was utilized to create a grid of horizontal and vertical scratches on the endothelial cell culture dish. The intersection points of the scratches served as coordinates to conveniently record each scratch's location. Loose cells were gently rinsed off with PBS and the medium was replaced with basic medium. Subsequently, the supernatant from the treated neutrophils was added to the endothelial cell culture medium. Scratch repair at the same location was documented at 0 and 24 hours post-treatment using an inverted microscope. The width of the scratches was analyzed using Image J software to assess the migratory capacity of the endothelial cells.

5.15. Western blot test

To evaluate the influence of various piezoelectric films on neutrophil traps, neutrophils treated with these films were centrifuged to yield their total protein content. Following quantitative electrophoresis, the proteins were transferred onto a PVDF membrane. This membrane was then blocked using 5% skim milk and incubated with specific antibodies. Protein expression was subsequently determined via a chemiluminescent technique. ImageJ was utilized for the processing of grayscale value data, and the expression level of the target protein was normalized accordingly. The primary antibodies employed included Histone H3 (1:1000, AB281584, abcam, UK) and β -actin (1:5000, LF201, Epizyme, China). The secondary antibodies used were HRP-labeled Goat Anti-Mouse IgG (1:10000, LF 101, Epizyme, China) and HRP-labeled Goat Anti-Rabbit IgG (1:10000, LF 102, Epizyme, China).

5.16. Animal surgeries and procedures

The male Sprague-Dawley rats utilized in this study were sourced from the Laboratory Animal Center of Shanghai Sixth People's Hospital. All animal and experimental protocols were scrutinized and sanctioned by the Animal Experimental Ethics Committee of Shanghai Sixth People's Hospital. Five animals per group were procured from Xipulbikai Experimental Animal, Shanghai.

Rats were weighed to the nearest 0.1 grams and anesthetized via an intraperitoneal injection of sodium pentobarbital, dosed at 30 mg/kg of body weight. After a brief period of 5 minutes, the rats' muscles relaxed and both pain and corneal reflexes ceased. A surgical incision of 5cm was made on the right hind limb of each rat, which was in a prone position. The gluteus maximus muscle and deep fascia were delicately separated until the sciatic nerve was revealed. A portion of this nerve, measuring 10mm, was then excised. For the experimental groups, a nerve conduit, 12 mm in length, was used to bridge the severed nerve ends. The transected nerve was gingerly inserted 1mm into the nerve conduit and meticulously sutured with a 6-0 suture under microscopic observation. For the autogenous nerve transplantation group, the severed nerve was rotated 180° before suturing. The muscle and epidermis were then closed with a 4-0 suture. Post-operatively, the rats were warmed under a light until they regained consciousness.

5.17. Behavioral analysis

Following a recovery period of three months, we utilized a gait analyzer (VisuGait, XR-XFP101, China) to record the relative data pertaining to the rats' ambulatory trajectories. The rats were permitted to traverse

a secure, dimly lit tunnel with a pressure-sensitive, transparent acrylic sheet situated beneath. The unique characteristics of these plates ensured comprehensive recording of the rats' movements via an under-tunnel camera, while also transmitting data from their footprints to a connected computer. Quantitative evaluation of the Sciatic nerve recovery was conducted via the interactive paw print measurement module for the injured right hind limb. The footprint analysis machine automatically measures relevant parameters of the footprint and calculates the sciatic nerve function index (SFI), which range from 0 (indicating normal function) to 100 (denoting complete loss of function), based on the preset formula.

5.18. Electrophysiological Assessment

In alignment with the model, rats were anesthetized using sodium pentobarbital. Following anesthesia, the right hind limb of the rat was shaved. Subsequently, we reopened the nerve defect site, mirroring the original incision, thereby exposing the two severed nerve ends. Needle electrodes were then strategically implanted into the right gastrocnemius muscle of the rats, maintaining a consistent stimulation intensity and frequency of 20 ma and 1.5 Hz, respectively. Finally, the resultant electromyography (EMG) was meticulously recorded and analyzed utilizing Image J.

5.19. Hematologic evaluation

The rats were carefully positioned supine and secured. Following this, a dissection was performed along the anterior abdominal midline, involving the skin, fascia, and muscle. The abdominal cavity was subsequently exposed by delicately opening the intestines and passively separating the retroperitoneum, thereby revealing the abdominal aorta. Whole blood was then procured using a disposable blood collection needle and an anticoagulant blood collection vessel. Arterial blood was collected separately using an EP tube. After a waiting period of 30 minutes, centrifugation was applied to collect the serum. Both the whole blood and serum were then utilized to assess various physiological indicators.

5.20. Histological experiments

Following blood collection, the animals are euthanized via an overdose of anaesthetic. The sciatic nerve and muscles are harvested, alongside the heart, lungs, liver, spleen, and kidneys. It is crucial to mention that for paired organs, only the left side is procured, and in case of lobes, the largest lobe is chosen. The collected tissues are subsequently fixed at 4°C in 4% paraformaldehyde solution for 24 hours, following which paraffin-embedded sections are prepared on the next day. For Hematoxylin-Eosin (HE) staining, the sections are initially stained with hematoxylin, subsequently with eosin, and finally dehydrated and sealed. Myelin sheath thickness was determined by g-ratio analysis by dividing the axonal diameter by the fiber diameter (diameter of axon including the myelin sheath). For Masson staining, the sections undergo staining with potassium dichromate, Ponceau red, phosphomolybdic acid and aniline blue, followed by differentiation with glacial acetic acid. For immunofluorescence experiments, the chosen primary antibodies are Histone H3 (1:2000, AB281584, abcam) and Myeloperoxidase (1:50, AB300650, abcam), and the secondary antibodies are Abflo 488-conjugated Goat Anti-Rabbit IgG (1:200, AS053, ABclonal, China) and CY3 conjugated Goat Anti-Rat IgG (1:500, A0507, Beyotime, China).

5.21. Statistical analysis

The presented data are expressed as the mean \pm standard deviation, derived from at least three independent experiments. The determination of statistical significance was carried out using Student's t test or ANOVA, with Bonferroni correction applied to the P values.

Supporting Information

Supporting Information is available from the Wiley Online Library or from the author.

Acknowledgments

This work was supported by the National Key R&D Program of China (No. 2021YFC2400800), the Projects of the National Natural Science Foundation of China (Nos. 82072452, 82272475); the Science and Technology Commission of Shanghai Municipality (No. 20DZ2254900) ; the Sino-German Mobility Programme (No. M-0699); the Excellent Youth Cultivation Program of Shanghai Sixth People’s Hospital, No. ynyq202201; the Medical Engineering Co-Project of University of Shanghai for Science and Technology, 10-22-310-520; and a grant from Shanghai Municipal Health Commission, No. 202040399.

Conflicts of interest declaration

The authors declare no conflict of interest.

Data Availability Statement

All data that support the findings of this study are included in the paper and the Supporting Information. Additional data related to this paper are available from the corresponding author upon reasonable request.

Author Contribution

Y.L., X.Y., L.Z. and J.S. contributed equally to this work. Y.L. and L.Z. performed the experience and Y.L. drafted the manuscript. X.Y. and J.S. participated in the design of the experiment and reviewed the manuscript. Y.Q. reviewed the literature and commented on the manuscript. Y.O., Y.Q., and C.H. revised the manuscript. All authors read and approved the final version.

Received: ((will be filled in by the editorial staff))

Revised: ((will be filled in by the editorial staff))

Published online: ((will be filled in by the editorial staff))

References

- [1] J.W. Squair, M. Milano, A. de Coucy, M. Gautier, M.A. Skinnider, N.D. James, N. Cho, A. Lasne, C. Kathe, T.H. Hutson, S. Ceto, L. Baud, K. Galan, V. Aureli, A. Laskaratos, Q. Barraud, T.J. Deming, R.E. Kohman, B.L. Schneider, Z. He, J. Bloch, M.V. Sofroniew, G. Courtine, M.A. Anderson, Recovery of walking after paralysis by regenerating characterized neurons to their natural target region, *SCIENCE* 381(6664) (2023) 1338-1345.
- [2] F. Jin, T. Li, T. Yuan, L. Du, C. Lai, Q. Wu, Y. Zhao, F. Sun, L. Gu, T. Wang, Z.Q. Feng, Physiologically Self-Regulated, Fully Implantable, Battery-Free System for Peripheral Nerve Restoration, *Adv Mater* 33(48) (2021) e2104175.
- [3] J.C. Chen, P. Kan, Z. Yu, F. Alrashdan, R. Garcia, A. Singer, C.S.E. Lai, B. Avants, S. Crosby, Z. Li, B. Wang, M.M. Felicella, A. Robledo, A.V. Peterchev, S.M. Goetz, J.D. Hartgerink, S.A. Sheth, K. Yang, J.T. Robinson, A wireless millimetric magnetoelectric implant for the endovascular stimulation of peripheral nerves, *Nature Biomedical Engineering* 6(6) (2022) 706-716.

- [4] F. Jin, T. Li, Z. Wei, R. Xiong, L. Qian, J. Ma, T. Yuan, Q. Wu, C. Lai, X. Ma, F. Wang, Y. Zhao, F. Sun, T. Wang, Z.-Q. Feng, Biofeedback electrostimulation for bionic and long-lasting neural modulation, *Nature Communications* 13(1) (2022).
- [5] J. Li, L. Kang, Y. Yu, Y. Long, J.J. Jeffery, W. Cai, X. Wang, Study of long-term biocompatibility and bio-safety of implantable nanogenerators, *Nano Energy* 51 (2018) 728-735.
- [6] B. Chu, X. Qin, Q. Zhu, H. Wang, Z. Wen, X. Sun, Y. He, S.-T. Lee, Triboelectric current stimulation alleviates in vitro cell migration and in vivo tumor metastasis, *Nano Energy* 100 (2022).
- [7] Z. Liu, X. Wan, Z.L. Wang, L. Li, Electroactive Biomaterials and Systems for Cell Fate Determination and Tissue Regeneration: Design and Applications, *Adv Mater* 33(32) (2021) e2007429.
- [8] X. Wang, J. Song, J. Liu, Z.L. Wang, Direct-current nanogenerator driven by ultrasonic waves, *SCIENCE* 316(5821) (2007) 102-5.
- [9] D.K. Piech, B.C. Johnson, K. Shen, M.M. Ghanbari, K.Y. Li, R.M. Neely, J.E. Kay, J.M. Carmena, M.M. Maharbiz, R. Muller, A wireless millimetre-scale implantable neural stimulator with ultrasonically powered bidirectional communication, *Nature Biomedical Engineering* 4(2) (2020) 207-222.
- [10] M. Zhou, M. Huang, H. Zhong, C. Xing, Y. An, R. Zhu, Z. Jia, H. Qu, S. Zhu, S. Liu, L. Wang, H. Ma, Z. Qu, G. Ning, S. Feng, Contact Separation Triboelectric Nanogenerator Based Neural Interfacing for Effective Sciatic Nerve Restoration, *ADVANCED FUNCTIONAL MATERIALS* 32(22) (2022).
- [11] S.K. Karan, S. Maiti, J.H. Lee, Y.K. Mishra, B.B. Khatua, J.K. Kim, Recent Advances in Self-Powered Tribo-/Piezoelectric Energy Harvesters: All-In-One Package for Future Smart Technologies, *ADVANCED FUNCTIONAL MATERIALS* 30(48) (2020).
- [12] Z. Li, G. Zhu, R. Yang, A.C. Wang, Z.L. Wang, Muscle-driven in vivo nanogenerator, *Adv Mater* 22(23) (2010) 2534-7.
- [13] A.L. Cattin, J.J. Burden, L. Van Emmenis, F.E. Mackenzie, J.J. Hoving, N. Garcia Calavia, Y. Guo, M. McLaughlin, L.H. Rosenberg, V. Quereda, D. Jamecna, I. Napoli, S. Parrinello, T. Enver, C. Ruhrberg, A.C. Lloyd, Macrophage-Induced Blood Vessels Guide Schwann Cell-Mediated Regeneration of Peripheral Nerves, *CELL* 162(5) (2015) 1127-39.
- [14] G. Murillo, A. Blanquer, C. Vargas-Estevez, L. Barrios, E. Ibanez, C. Nogues, J. Esteve, Electromechanical Nanogenerator-Cell Interaction Modulates Cell Activity, *ADVANCED MATERIALS* 29(24) (2017).
- [15] J. Tian, R. Shi, Z. Liu, H. Ouyang, M. Yu, C. Zhao, Y. Zou, D. Jiang, J. Zhang, Z. Li, Self-powered implantable electrical stimulator for osteoblasts' proliferation and differentiation, *Nano Energy* 59 (2019) 705-714.
- [16] W. Deng, Y. Zhou, A. Libanori, G. Chen, W. Yang, J. Chen, Piezoelectric nanogenerators for personalized healthcare, *CHEMICAL SOCIETY REVIEWS* 51(9) (2022) 3380-3435.
- [17] Y. Park, Y.E. Shin, J. Park, Y. Lee, M.P. Kim, Y.R. Kim, S. Na, S.K. Ghosh, H. Ko, Ferroelectric Multilayer Nanocomposites with Polarization and Stress Concentration Structures for Enhanced Triboelectric Performances, *ACS Nano* 14(6) (2020) 7101-7110.
- [18] Z. Yin, B. Tian, Q. Zhu, C. Duan, Characterization and Application of PVDF and Its Copolymer Films Prepared by Spin-Coating and Langmuir-Blodgett Method, *Polymers (Basel)* 11(12) (2019).
- [19] H. Abdolmaleki, A.B. Haugen, K.B. Buhl, K. Daasbjerg, S. Agarwala, Interfacial Engineering of PVDF-TrFE toward Higher Piezoelectric, Ferroelectric, and Dielectric Performance for Sensing and Energy Harvesting Applications, *Adv Sci (Weinh)* (2023) e2205942.
- [20] O. Gryshkov, F. Al Halabi, A.I. Kuhn, S. Leal-Marín, L.J. Freund, M. Forthmann, N. Meier, S.A. Barker, K. Haastert-Talini, B. Glasmacher, PVDF and P(VDF-TrFE) Electrospun Scaffolds for Nerve Graft

Engineering: A Comparative Study on Piezoelectric and Structural Properties, and In Vitro Biocompatibility, *Int J Mol Sci* 22(21) (2021).

[21] A. Wang, Z. Liu, M. Hu, C. Wang, X. Zhang, B. Shi, Y. Fan, Y. Cui, Z. Li, K. Ren, Piezoelectric nanofibrous scaffolds as in vivo energy harvesters for modifying fibroblast alignment and proliferation in wound healing, *Nano Energy* 43 (2018) 63-71.

[22] Y.P. Lim, J.S.C. Koay, J. Zhao, S. Huang, B.T. Goh, K.C. Aw, B. Chen, C.Y. Haw, W.C. Gan, Modulating ZnO Growth Structures for Maximum Power Output of Hybrid Piezo/Triboelectric Nanogenerator, *ADVANCED FUNCTIONAL MATERIALS* 32(46) (2022).

[23] X. Yao, Z. Yan, A. Liu, L. Zhan, Y. Liu, C. Huang, Y. Ouyang, H. Ruan, Y. Qian, C. Fan, Metal organic framework-modified bioadaptable implant potentiates the reconstruction of nerve microenvironment via immunometabolism reprogramming, *Nano Today* 49 (2023).

[24] X. Wan, X. Zhang, Z. Liu, J. Zhang, Z. Li, Z.L. Wang, L. Li, Noninvasive manipulation of cell adhesion for cell harvesting with piezoelectric composite film, *Applied Materials Today* 25 (2021).

[25] Y. Qian, H. Lin, Z. Yan, J. Shi, C. Fan, Functional nanomaterials in peripheral nerve regeneration: Scaffold design, chemical principles and microenvironmental remodeling, *Materials Today* 51 (2021) 165-187.

[26] P. Yang, Y. Peng, X. Dai, J. Jie, D. Kong, X. Gu, Y. Yang, Bionic peptide scaffold in situ polarization and recruitment of M2 macrophages to promote peripheral nerve regeneration, *Bioactive Materials* 30 (2023) 85-97.

[27] L. Zeboudj, G. Sideris-Lampretsas, R. Silva, S. Al-Mударis, F. Picco, S. Fox, D. Chambers, M. Malcangio, Silencing miR-21-5p in sensory neurons reverses neuropathic allodynia via activation of TGF- β -related pathway in macrophages, *J Clin Invest* 133(11) (2023).

[28] T. Tanaka, H. Okuda, A. Isonishi, Y. Terada, M. Kitabatake, T. Shinjo, K. Nishimura, S. Takemura, H. Furue, T. Ito, K. Tatsumi, A. Wanaka, Dermal macrophages set pain sensitivity by modulating the amount of tissue NGF through an SNX25-Nrf2 pathway, *Nat Immunol* 24(3) (2023) 439-451.

[29] J.M. Adrover, A. Aroca-Crevillen, G. Crainiciuc, F. Ostos, Y. Rojas-Vega, A. Rubio-Ponce, C. Cilloniz, E. Bonzon-Kulichenko, E. Calvo, D. Rico, M.A. Moro, C. Weber, I. Lizasoain, A. Torres, J. Ruiz-Cabello, J. Vazquez, A. Hidalgo, Programmed 'disarming' of the neutrophil proteome reduces the magnitude of inflammation, *Nat Immunol* 21(2) (2020) 135-144.

[30] G. Wigerblad, M.J. Kaplan, Neutrophil extracellular traps in systemic autoimmune and autoinflammatory diseases, *Nat Rev Immunol* 23(5) (2023) 274-288.

[31] Y. Yamamoto, K. Kadoya, M.A. Terkawi, T. Endo, K. Konno, M. Watanabe, S. Ichihara, A. Hara, K. Kaneko, N. Iwasaki, M. Ishijima, Neutrophils delay repair process in Wallerian degeneration by releasing NETs outside the parenchyma, *Life Sci Alliance* 5(10) (2022).

[32] S.L. Wong, M. Demers, K. Martinod, M. Gallant, Y. Wang, A.B. Goldfine, C.R. Kahn, D.D. Wagner, Diabetes primes neutrophils to undergo NETosis, which impairs wound healing, *Nat Med* 21(7) (2015) 815-9.

[33] J. Wang, H. Wang, X. Mo, H. Wang, Reduced Graphene Oxide-Encapsulated Microfiber Patterns Enable Controllable Formation of Neuronal-Like Networks, *ADVANCED MATERIALS* 32(40) (2020).

[34] X. Yao, L. Zhan, Z. Yan, J. Li, L. Kong, X. Wang, H. Xiao, H. Jiang, C. Huang, Y. Ouyang, Y. Qian, C. Fan, Non-electric bioelectrical analog strategy by a biophysical-driven nano-micro spatial anisotropic scaffold for regulating stem cell niche and tissue regeneration in a neuronal therapy, *Bioactive Materials* 20 (2023) 319-338.

[35] Z. Yan, T. Ye, L. Yang, H. Jiang, C. Chen, S. Chen, Y. Qian, C. Fan, Nanobiology Dependent Therapeutic Convergence between Biocompatibility and Bioeffectiveness of Graphene Oxide Quantum Dot Scaffold

for Immuno-Inductive Angiogenesis and Nerve Regeneration, *ADVANCED FUNCTIONAL MATERIALS* 33(9) (2023).

[36] X. Zhang, L. Li, J. Ouyang, L. Zhang, J. Xue, H. Zhang, W. Tao, Electroactive electrospun nanofibers for tissue engineering, *Nano Today* 39 (2021).

[37] W. Liu, H. Zhao, C. Zhang, S. Xu, F. Zhang, L. Wei, F. Zhu, Y. Chen, Y. Chen, Y. Huang, M. Xu, Y. He, B.C. Heng, J. Zhang, Y. Shen, X. Zhang, H. Huang, L. Chen, X. Deng, In situ activation of flexible magnetoelectric membrane enhances bone defect repair, *Nature Communications* 14(1) (2023).

[38] J.C. Chen, G. Bhave, F. Alrashdan, A. Dhuliyawalla, K.J. Hogan, A.G. Mikos, J.T. Robinson, Self-rectifying magnetoelectric metamaterials for remote neural stimulation and motor function restoration, *NATURE MATERIALS* (2023).

[39] E. Elsanadidy, I.M. Mosa, D. Luo, X. Xiao, J. Chen, Z.L. Wang, J.F. Rusling, Advances in Triboelectric Nanogenerators for Self-powered Neuromodulation, *ADVANCED FUNCTIONAL MATERIALS* 33(8) (2023).

[40] T. Xie, Q. Liu, G. Xue, Y. Zhang, J. Zhou, Z. Zhu, X. Gou, Experimental-numerical analysis of cell adhesion-mediated electromechanical stimulation on piezoelectric nanofiber scaffolds, *J Biomech* 129 (2021) 110777.

[41] R. Mao, B. Yu, J. Cui, Z. Wang, X. Huang, H. Yu, K. Lin, S.G.F. Shen, Piezoelectric stimulation from electrospun composite nanofibers for rapid peripheral nerve regeneration, *Nano Energy* 98 (2022).

[42] J. Nunes-Pereira, V. Sencadas, V. Correia, J.G. Rocha, S. Lanceros-Méndez, Energy harvesting performance of piezoelectric electrospun polymer fibers and polymer/ceramic composites, *Sensors and Actuators A: Physical* 196 (2013) 55-62.

[43] Y.C. Yun Qian, Jiangyu Cai, Xiaotian Zhao, Yuanming Ouyang, Wei-En Yuan, Cunyi Fan., Advances in electrical and magnetic stimulation on nerve regeneration, *Regenerative Medicine* (2019).

[44] D. Jeong, J. Lee, Y.-S. Yi, Y. Yang, K.W. Kim, J.Y. Cho, p38/AP-1 Pathway in Lipopolysaccharide-Induced Inflammatory Responses Is Negatively Modulated by Electrical Stimulation, *MEDIATORS OF INFLAMMATION* 2013 (2013) 1-11.

[45] L. Yang, Q. Liu, X. Zhang, X. Liu, B. Zhou, J. Chen, D. Huang, J. Li, H. Li, F. Chen, J. Liu, Y. Xing, X. Chen, S. Su, E. Song, DNA of neutrophil extracellular traps promotes cancer metastasis via CCDC25, *NATURE* 583(7814) (2020) 133-138.

[46] A. Mousset, E. Lecorgne, I. Bourget, P. Lopez, K. Jenovai, J. Cherfils-Vicini, C. Dominici, G. Rios, C. Girard-Riboulleau, B. Liu, D.L. Spector, S. Ehmsen, S. Renault, C. Hego, F. Mechta-Grigoriou, F.-C. Bidard, M.G. Terp, M. Egeblad, C. Gaggioli, J. Albregues, Neutrophil extracellular traps formed during chemotherapy confer treatment resistance via TGF- β activation, *CANCER CELL* 41(4) (2023) 757-775.e10.

[47] I.L. Linde, T.R. Prestwood, J. Qiu, G. Pilarowski, M.H. Linde, X. Zhang, L. Shen, N.E. Reticker-Flynn, D.K.-C. Chiu, L.Y. Sheu, S. Van Deursen, L.L. Tolentino, W.-C. Song, E.G. Engleman, Neutrophil-activating therapy for the treatment of cancer, *CANCER CELL* 41(2) (2023) 356-372.e10.

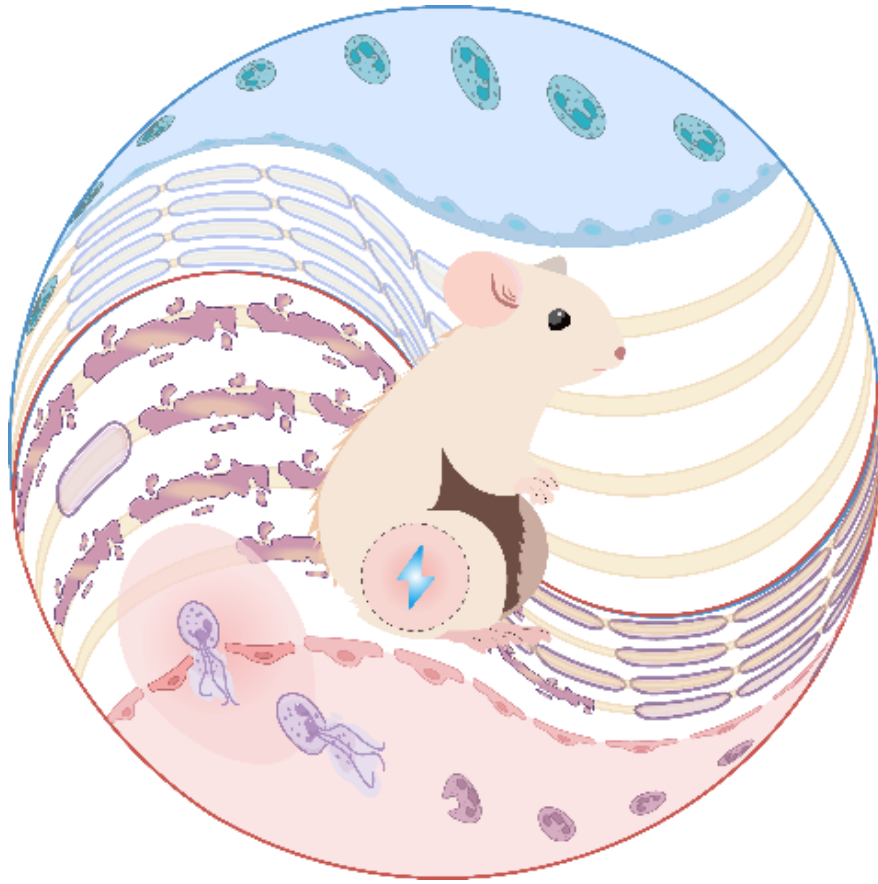
[48] S. Shen, X. Cheng, L. Zhou, Y. Zhao, H. Wang, J. Zhang, X. Sun, Y. Wang, Y. Shu, Y. Xu, Y. Tao, M. Li, Z. Lu, W. Cai, G. Nie, W. Qiu, Neutrophil Nanovesicle Protects against Experimental Autoimmune Encephalomyelitis through Enhancing Myelin Clearance by Microglia, *ACS Nano* 16(11) (2022) 18886-18897.

[49] J.A. Lindborg, M. Mack, R.E. Zigmond, Neutrophils Are Critical for Myelin Removal in a Peripheral Nerve Injury Model of Wallerian Degeneration, *J Neurosci* 37(43) (2017) 10258-10277.

[50] M. Nahrendorf, F.K. Swirski, Immunology. Neutrophil-macrophage communication in inflammation and atherosclerosis, *SCIENCE* 349(6245) (2015) 237-8.

- [51] M.S.F. Ng, I. Kwok, L. Tan, C. Shi, D. Cerezo-Wallis, Y. Tan, K. Leong, G.F. Calvo, K. Yang, Y. Zhang, J. Jin, K.H. Liong, D. Wu, R. He, D. Liu, Y.C. Teh, C. Bleriot, N. Caronni, Z. Liu, K. Duan, V. Narang, I. Ballesteros, F. Moalli, M. Li, J. Chen, Y. Liu, L. Liu, J. Qi, Y. Liu, L. Jiang, B. Shen, H. Cheng, T. Cheng, V. Angeli, A. Sharma, Y.-h. Loh, H.L. Tey, S.Z. Chong, M. Iannacone, R. Ostuni, A. Hidalgo, F. Ginhoux, L.G. Ng, Deterministic reprogramming of neutrophils within tumors, *SCIENCE* 383(6679) (2024) eadf6493.
- [52] R. Wang, Y. Zhu, Z. Liu, L. Chang, X. Bai, L. Kang, Y. Cao, X. Yang, H. Yu, M.J. Shi, Y. Hu, W. Fan, B.Q. Zhao, Neutrophil extracellular traps promote tPA-induced brain hemorrhage via cGAS in mice with stroke, *BLOOD* 138(1) (2021) 91-103.
- [53] M. Yang, H. Jiang, C. Ding, L. Zhang, N. Ding, G. Li, F. Zhang, J. Wang, L. Deng, J. Liu, Y. Xu, STING activation in platelets aggravates septic thrombosis by enhancing platelet activation and granule secretion, *IMMUNITY* 56(5) (2023) 1013-1026.e6.
- [54] X. Wang, C. Yang, X. Wang, J. Miao, W. Chen, Y. Zhou, Y. Xu, Y. An, A. Cheng, W. Ye, M. Chen, D. Song, X. Yuan, J. Wang, P. Qian, A.R. Wu, Z.-Y. Zhang, K. Liu, Driving axon regeneration by orchestrating neuronal and non-neuronal innate immune responses via the IFN γ -cGAS-STING axis, *NEURON* 111(2) (2023) 236-255.e7.
- [55] J.A. Orkwis, A.K. Wolf, Z.J. Mularczyk, A.E. Bryan, C.S. Smith, R. Brown, M. Krutko, A. McCann, R.M. Collar, L. Esfandiari, G.M. Harris, Mechanical stimulation of a bioactive, functionalized PVDF-TrFE scaffold provides electrical signaling for nerve repair applications, *Biomater Adv* 140 (2022) 213081.
- [56] X. Zhang, X. Cui, D. Wang, S. Wang, Z. Liu, G. Zhao, Y. Zhang, Z. Li, Z.L. Wang, L. Li, Piezo-electric Nanotopography Induced Neuron-Like Differentiation of Stem Cells, *ADVANCED FUNCTIONAL MATERIALS* 29(22) (2019).
- [57] Y. Qian, Y. Xu, Z. Yan, Y. Jin, X. Chen, W.-E. Yuan, C. Fan, Boron nitride nanosheets functionalized channel scaffold favors microenvironment rebalance cocktail therapy for piezocatalytic neuronal repair, *Nano Energy* 83 (2021).
- [58] X.Y. Yao, Y. Qian, C.Y. Fan, Electroactive nanomaterials in the peripheral nerve regeneration, *J Mater Chem B* 9(35) (2021) 6958-6972.
- [59] K. Kostarelos, M. Vincent, C. Hebert, J.A. Garrido, Graphene in the Design and Engineering of Next-Generation Neural Interfaces, *ADVANCED MATERIALS* 29(42) (2017).
- [60] L.A.L. Tang, W.C. Lee, H. Shi, E.Y.L. Wong, A. Sadovoy, S. Gorelik, J. Hopley, C.T. Lim, K.P. Loh, Highly Wrinkled Cross-Linked Graphene Oxide Membranes for Biological and Charge-Storage Applications, *Small* 8(3) (2011) 423-431.
- [61] S. Tonello, M. Rizzi, M. Migliario, V. Rocchetti, F. Renò, Low concentrations of neutrophil extracellular traps induce proliferation in human keratinocytes via NF- κ B activation, *J Dermatol Sci* 88(1) (2017) 110-116.
- [62] A.R. Sas, K.S. Carbajal, A.D. Jerome, R. Menon, C. Yoon, A.L. Kalinski, R.J. Giger, B.M. Segal, A new neutrophil subset promotes CNS neuron survival and axon regeneration, *Nat Immunol* 21(12) (2020) 1496-1505.
- [63] M. Palomino-Segura, J. Sicilia, I. Ballesteros, A. Hidalgo, Strategies of neutrophil diversification, *Nat Immunol* 24(4) (2023) 575-584.
- [64] I. Arnaoutova, H.K. Kleinman, In vitro angiogenesis: endothelial cell tube formation on gelled basement membrane extract, *Nature Protocols* 5(4) (2010) 628-635.

ToC Figure



Hosted file

figures.docx available at <https://authorea.com/users/777373/articles/902744-mechanical-cellular-electrical-conversion-model-reshapes-the-immune-microenvironment-of-peripheral-nerve-by-modulating-neutrophil-extracellular-traps>